

CYSRT1: An Antimicrobial Epidermal Protein that Can Interact with Late Cornified Envelope Proteins

JID Open



Hanna Niehues¹, Gijs Rikken¹, Ferry F.J. Kersten¹, Jorine M. Eeftens²,
Ivonne M.J.J. van Vlijmen-Willems¹, Diana Rodijk-Olthuis¹, Patrick A.M. Jansen¹,
Wiljan J.A.J. Hendriks³, Thomas H.A. Ederveen⁴, Joost Schalkwijk¹, Ellen H. van den Bogaard^{1,5} and
Patrick L.J.M. Zeeuwen^{1,5}

Late cornified envelope (LCE) proteins are small cationic epidermal proteins with antimicrobial properties, and the combined deletion of *LCE3B* and *LCE3C* genes is a risk factor for psoriasis that affects skin microbiome composition. In a yeast two-hybrid screen, we identified CYSRT1 as an interacting partner of members of all LCE groups except LCE6. These interactions were confirmed in a mammalian cell system by coimmunoprecipitation. CYSRT1 is a protein of unknown function that is specifically expressed in cutaneous and oral epithelia and spatially colocalizes with LCE proteins in the upper layers of the suprabasal epidermis. Constitutive CYSRT1 expression is present in fully differentiated epidermis and can be further induced *in vivo* by disruption of the skin barrier upon stratum corneum removal. Transcriptional regulation correlates to keratinocyte terminal differentiation but not to skin bacteria exposure. Similar to LCEs, CYSRT1 was found to have antibacterial activity against *Pseudomonas aeruginosa*. Comparative gene sequence analysis and protein amino acid alignment indicate that CYSRT1 is highly conserved among vertebrates and has putative antimicrobial activity. To summarize, we identified CYSRT1 in the outer skin layer, where it colocalizes with LCE proteins and contributes to the constitutive epidermal antimicrobial host defense repertoire.

Journal of Investigative Dermatology (2023) **143**, 1498–1508; doi:10.1016/j.jid.2023.01.022

INTRODUCTION

Over the last two decades, a large number of epidermal antimicrobial proteins (AMPs) have been identified such as defensins, such as human β -defensin-2 (Harder et al., 1997; Liu et al., 1998), cathelicidins (Frohm et al., 1997; Marchini et al., 2002), secretory leukocyte proteinase inhibitor/skin-derived antileukoprotease (Hiemstra et al., 1996; Sallenave et al., 1992), dermcidin (Schittek et al., 2001), and members of the S100 protein family (Büchau et al., 2007; Gläser et al., 2005). These AMPs, which are mostly produced in the stratum granulosum and deposited in the stratum corneum, provide protection against exogenous microbes as the first line of defense on the most outer part of our skin.

Recently, we reported that late cornified envelope (LCE) proteins, previously considered as terminal differentiation proteins contributing to stratum corneum barrier properties, possess antimicrobial activity. These LCEs are small cationic keratinocyte (KC)-expressed peptides having a broad-spectrum antimicrobial activity (Niehues et al., 2022, 2017). Similarly, other constituents of the cornified envelope have been found to be antimicrobial such as hornerin and FLG2 (Gerstel et al., 2018; Hansmann et al., 2015) and are classified as cationic intrinsically disordered antimicrobial peptides (CIDAMPs) (Latendorf et al., 2019). CIDAMPs, including LCEs, have strong antimicrobial activity independent of their amino acid sequence. Instead, AMP activity depends on a high content of disorder-promoting amino acids in linear cationic peptides as well as peptide chain length, net charge, lipidation, and environmental conditions. The presence of a multitude of CIDAMPs in the stratum corneum provides evidence for a much broader array of constitutively expressed AMPs in the skin than previously thought, which may impact the cutaneous microbiota composition.

Several skin diseases are linked to changes in cutaneous microbiota composition that could be linked to altered expression profiles of epidermal AMPs. Ichthyosis vulgaris is caused by homozygous loss of *FLG* (Smith et al., 2006), and *FLG* variations are the major risk factor for developing atopic dermatitis (Palmer et al., 2006). Both diseases are characterized by skin microbiome dysbiosis (Fyhrquist et al., 2019; Kong et al., 2012; Zeeuwen et al., 2017). *FLG* also has intrinsically disordered regions and is therefore considered a

¹Department of Dermatology, Radboud University Nijmegen Medical Center (Radboudumc), Nijmegen, The Netherlands; ²Department of Cell Biology, Faculty of Science, Radboud University, Nijmegen, The Netherlands; ³Department of Cell Biology, Radboud University Nijmegen Medical Center (Radboudumc), Nijmegen, The Netherlands; and ⁴Center for Molecular and Biomolecular Informatics (CMBI), Radboud University Nijmegen Medical Center (Radboudumc), Nijmegen, The Netherlands

⁵These authors contributed equally as senior authors.

Correspondence: Hanna Niehues, Department of Dermatology, Radboud University Nijmegen Medical Center (Radboudumc), PO BOX 9101, 6500 HB Nijmegen, The Netherlands. E-mail: Hanna.Niehues@radboudumc.nl

Abbreviations: AHR, aryl hydrocarbon receptor; AMP, antimicrobial protein; CIDAMP, cationic intrinsically disordered antimicrobial peptide; Co-IP, coimmunoprecipitation; HEE, human epidermal equivalent; KC, keratinocyte; LCE, late cornified envelope; Y2H, yeast two-hybrid

Received 14 June 2022; revised 21 December 2022; accepted 4 January 2023; accepted manuscript published online 15 February 2023; corrected proof published online 29 March 2023

potential CIDAMP (Latendorf et al., 2019). Moreover, copy number variation in the AMP-encoding gene *DEFB4* (Hollox et al., 2008) and insertion/deletion variation in *LCE* genes (*LCE3B/C_del*) (Bergboer et al., 2012; de Cid et al., 2009; Hüffmeier et al., 2010) contribute to the risk of developing psoriasis. Emerging evidence is found for microbiome dysbiosis in psoriasis; however, published data showed conflicting results regarding bacterial communities (Chang et al., 2018; Fyrquist et al., 2019). Nevertheless, we recently showed that the psoriasis risk factor deletion of *LCE3B/C* genes affects microbiota composition in healthy individuals (Niehues et al., 2022).

Identification of protein–protein interactions is a powerful way to understand protein function and contributes to our understanding of how dysregulation of these interactions, for example, owing to gene mutations or (post)transcriptional modifications, can contribute to disease. In this study, we screened for binding partners of LCE proteins within the complex network of stratum corneum proteins to determine interactions with skin-specific proteins that attribute to skin barrier function or host defense. We identified CYSRT1 as an interaction partner of LCE proteins using yeast two-hybrid (Y2H) screening and coimmunoprecipitation (Co-IP) and investigated the expression, regulation, and function of CYSRT1 in the epidermis.

RESULTS

CYSRT1 is an interacting partner for LCE proteins in vitro

To identify the interaction partners of LCE3 family proteins, we performed a GAL4-based interaction screen in yeast. We screened (Y2H) a human epidermis cDNA library for potential interactors of full-length LCE3A, LCE3B, and LCE3C. The PJ69-4A yeast strain was transformed with a DNA bait construct and first tested to exclude autoactivation. All three LCE3 family proteins were found to interact with several other proteins (Table 1). Among them, we identified CYSRT1, previously known as C9orf169, as a potential interaction partner of LCE3A, LCE3B, and LCE3C. In total, 13 different prey clones encoding CYSRT1 fragments were identified. We also screened our library with CYSRT1 itself and found the LCE3A protein, among other candidates (e.g., skin-derived antileukoprotease/elafin, human β -defensin-2, keratin 6, cornifelin), as a potential interaction partner (Supplementary Table S1). The LCE–CYSRT1 interaction was confirmed in a dedicated yeast 1-to-1 analysis in which CYSRT1 was expressed with different LCE genes, and protein–protein interactions were indicated by reporter gene activation (Supplementary Figure S1). This analysis confirmed the interaction between CYSRT1 and LCE3A and LCE3B (and a weaker interaction with LCE3C), and interestingly, we also found interactions between CYSRT1 and members of all other LCE protein groups, except for LCE6A. The interactions between CYSRT1 and other candidates (skin-derived antileukoprotease/elafin, human β -defensin-2, keratin 6, cornifelin) could not be confirmed in the yeast 1-to-1 screen (Supplementary Figure S1) and were therefore excluded from further analysis. Next, the LCE–CYSRT1 interaction was validated in a mammalian in vitro cell system by Co-IP of lysates from human embryonic kidney 293T cells in which HA-tagged CYSRT1 was cotransfected with FLAG-tagged LCE proteins. We found that all

Table 1. Identified LCE3A/B/C Interaction Partners from Yeast Two-Hybrid Screen

| LCE3 Protein | LCE Interactor (HUGO Gene Name) | Number Identified Clones |
|--------------|---------------------------------|--------------------------|
| LCE3A | GRN ¹ | 10 |
| LCE3B | | 3 |
| LCE3C | | 13 |
| LCE3A | CYSRT1 | 5 |
| LCE3B | | 6 |
| LCE3C | | 2 |
| LCE3A | NOTCH2NL | 2 |
| LCE3A | C1ORF68 | 2 |
| LCE3A | GLTSCR2 | 1 |
| LCE3A | TGM1 | 1 |
| LCE3B | LCE3A | 3 |
| LCE3B | LCE1B | 1 |
| LCE3B | LCE2C | 1 |
| LCE3B | LCE3E | 1 |
| LCE3B | HRG | 1 |

Abbreviations: GRN, Granulin; HRG, histidine-rich glycoprotein; HUGO, Human Genome Organisation; LCE, late cornified envelope.

¹Despite the large number of colonies identified, we did not proceed with GRN because this identified interaction partner was suspected to be false positive (most clones were not in frame with the GAL4-AD coding sequences).

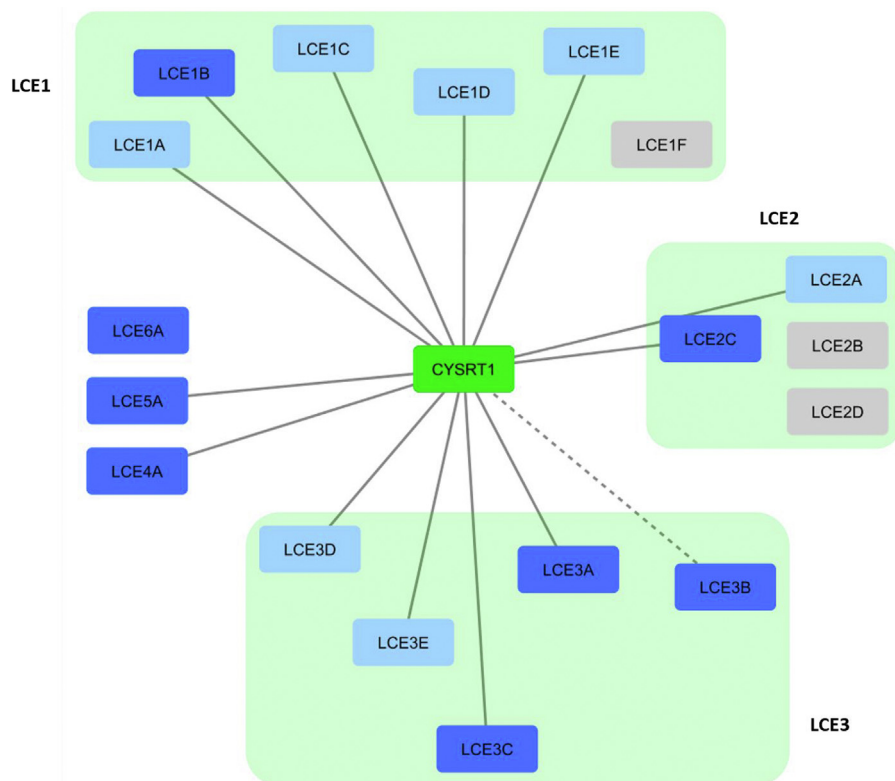
FLAG-tagged LCE proteins tested, except LCE6A and LCE3B (the latter only showing a faint signal), were coimmunoprecipitated with HA-tagged CYSRT1 (Supplementary Figure S2). Protein–protein interactions between CYSRT1 and LCE proteins that could be validated with the different techniques are schematically visualized in Figure 1.

CYSRT1 is expressed in skin and epithelial tissues

Considering the unknown biology and function of CYSRT1, we started a detailed investigation of its expression profiles and possible function. CYSRT1 is highly conserved among primates, rodents, laurasiatherian mammals, and marsupials (Supplementary Figure S3). According to the Ensemble database, CYSRT1 (Ensemble gene identification ENSG00000197191) exists as two predicted splice variants—one of 144 amino acids (accession number A8MQ03 in the Uniprot database) and one of 184 amino acids (accession number B8A4K4)—with theoretical molecular weights of 15.3 and 19.7 kDa, respectively. We detected endogenously expressed CYSRT1 derived from KC cell extracts derived from human epidermal equivalents (HEEs) as well as interfollicular epidermis as an approximately 18–20 kDa immunoreactive protein on western blots (Supplementary Figure S4). Gene expression analysis on a large panel of human tissues, including diverse epithelia, revealed that *CYSRT1* mRNA is mainly expressed in skin and oral epithelia (Figure 2a), which was confirmed at the protein level (Figure 2b). We observed a variation in CYSRT1 expression between different individuals. Some skin biopsies showed continuous CYSRT1 expression throughout the granular layer, whereas some others showed a patchy, discontinuous staining pattern (Supplementary Figure S5). Immunofluorescence double and triple staining indicated that CYSRT1 colocalizes with LCE2 and LCE3 in the skin and with LCE3 in the tonsil epithelium (Supplementary Figure S6). Analysis of skin biopsies with confocal microscopy revealed a spatial (co)

Figure 1. Observed CYSRT1–LCE protein interactions.

protein interactions. Dark blue-colored blocks indicate interactions of CYSRT1 with LCE proteins that were detected in both Y2H (original assay and 1:1) and Co-IP experiments. CYSRT1–LCE6A interaction was not found for all different assays (no line). The dotted gray line indicates a two-hybrid interaction that was not confirmed by Co-IP. Light blue-colored blocks indicate CYSRT1–LCE interactions that were only observed with Co-IP. Gray boxes indicate the LCEs that failed to be expressed as FLAG-tagged proteins for Co-IP analysis. Co-IP, coimmunoprecipitation; LCE, late cornified envelope; Y2H, yeast two-hybrid.



localization of CYSRT1, LCE2, and LCE3 at the cell membrane of the last living cell layer of the stratum granulosum adjacent to the stratum corneum (Figure 2c).

CYSRT1 expression in inflammatory conditions

LCE3 expression levels are elevated in psoriasis and upon stimulation of *in vitro* organotypic skin models with psoriasis-associated cytokines (Bergboer et al., 2011). For *CYSRT1* gene expression, no differences were found between healthy skin and lesional skin of patients with atopic dermatitis and patients with psoriasis (Figure 3a), in contrast to CYSRT1 protein that was found to be increased in lesional skin, such as the LCE3 proteins (Figure 3b). To define the inflammatory environment that induces CYSRT1 upregulation, undifferentiated human KC monolayer cultures were stimulated with inflammatory skin disease–associated cytokines. The mixture of T helper 1 cytokines (Figure 3c) and most specifically IFN- γ (Figure 3d) but not classical T helper 2 and T helper 17 cytokines induced *CYSRT1* gene expression. However, IFN- γ stimulation of fully stratified organotypic HEEs failed to induce *CYSRT1* (Figure 3e). This is most likely because of the already higher constitutive *CYSRT1* levels in the stratified organotypic epidermis (RT-qPCR Ct-value = 23) than in the monolayer KC cultures (Ct value = 28).

CYSRT1 expression is associated with KC terminal differentiation

To further investigate the regulation of CYSRT1 expression, we took advantage of our knowledge of the interacting LCE3 proteins. Expression levels of the LCE3 family are upregulated upon skin barrier disruption (Bergboer et al., 2011; de

Koning et al., 2012; Niehues et al., 2016). Similar to the LCE proteins, CYSRT1 was significantly induced after tape stripping of normal, nonlesional psoriatic, and uninvolved atopic dermatitis skin and at similar levels between the two skin conditions (Figure 4a and b). This is most likely related to the induction of KC terminal differentiation as a physiological response after skin damage and not by exogenous (bacterial) triggers because we could not find evidence for *CYSRT1* gene regulation by skin bacteria (Figure 4c). Indeed, *CYSRT1* mRNA expression levels follow the dynamics of KC terminal differentiation over time (Figure 4d), reaching plateau protein levels in three-dimensional HEEs upon complete epidermal stratification (Figure 4e). Thereafter, upon terminal differentiation of all epidermal layers (during prolonged culture periods of 12–14 days at the air–liquid interface) and loss of the stratum granulosum, CYSRT1 expression ceases.

KC terminal differentiation is regulated by a plethora of transcription factors, including the aryl hydrocarbon receptor (AHR). Targeting this ligand-activated transcription factor with dermatological therapies such as coal tar or Tapinarof can drive epidermal differentiation and restore skin barrier defects (Bissonnette et al., 2021; Smith et al., 2017; van den Bogaard et al., 2021). Similar to other structural epidermal differentiation proteins (e.g., involucrin, loricrin) (van den Bogaard et al., 2015, 2013) and those with putative antimicrobial function (e.g., FLG, LCEs, hornerin) (Latendorf et al., 2019; Niehues et al., 2022; Smits et al., 2020), activation of the AHR signaling pathway (as indicated by the increased transcript levels for the AHR-target *CYP1A1*) (Figure 4f) upregulates *CYSRT1* gene expression (Figure 4g) in coal tar–treated monolayer KCs. In HEEs, epidermal CYSRT1

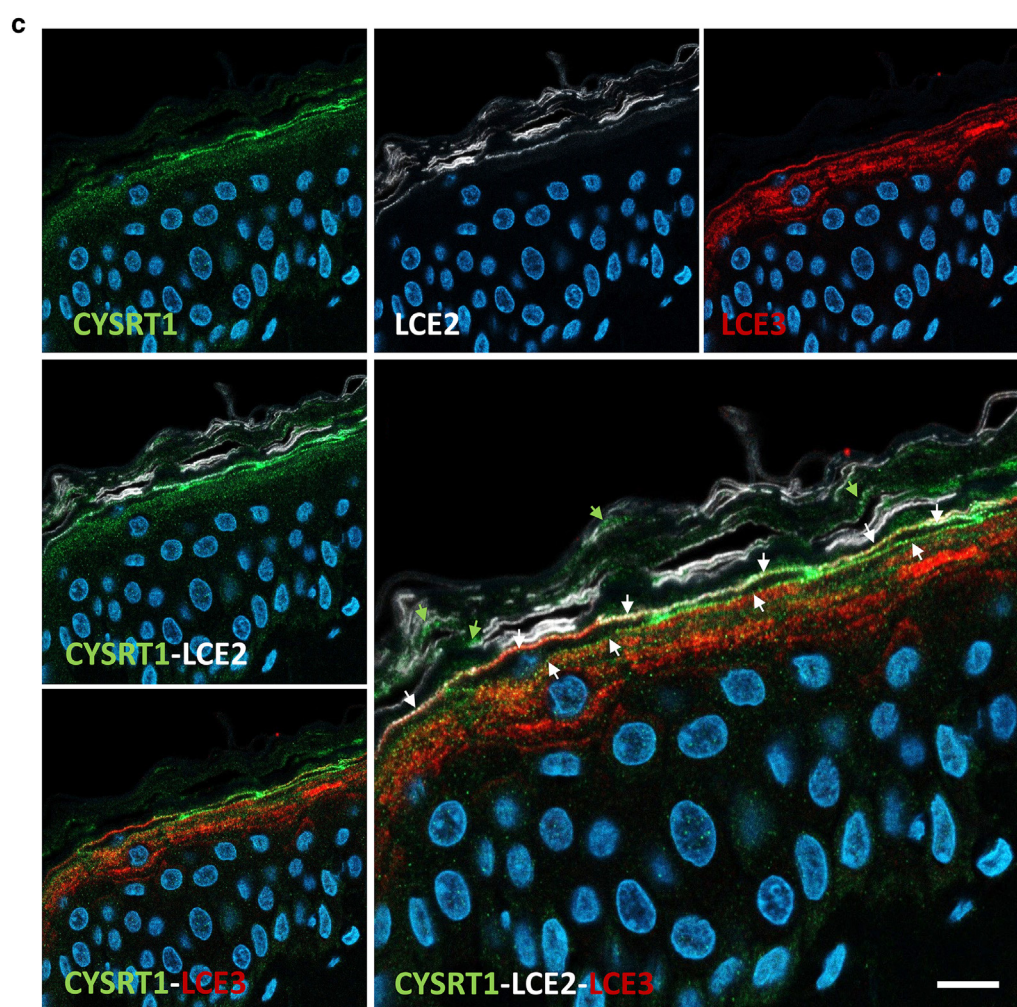
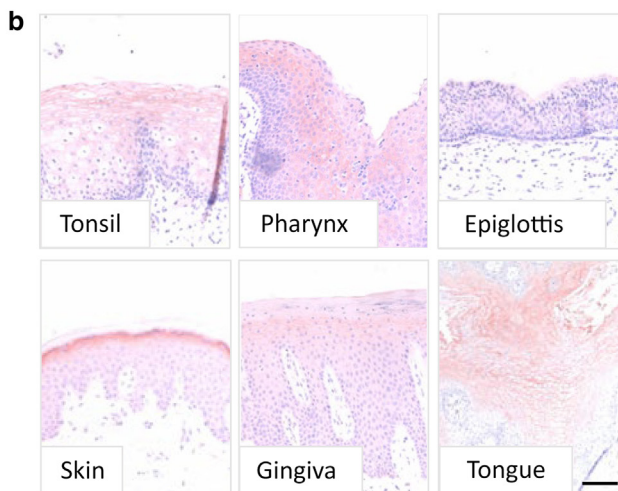
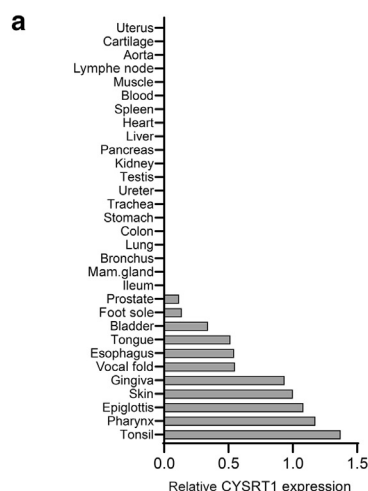
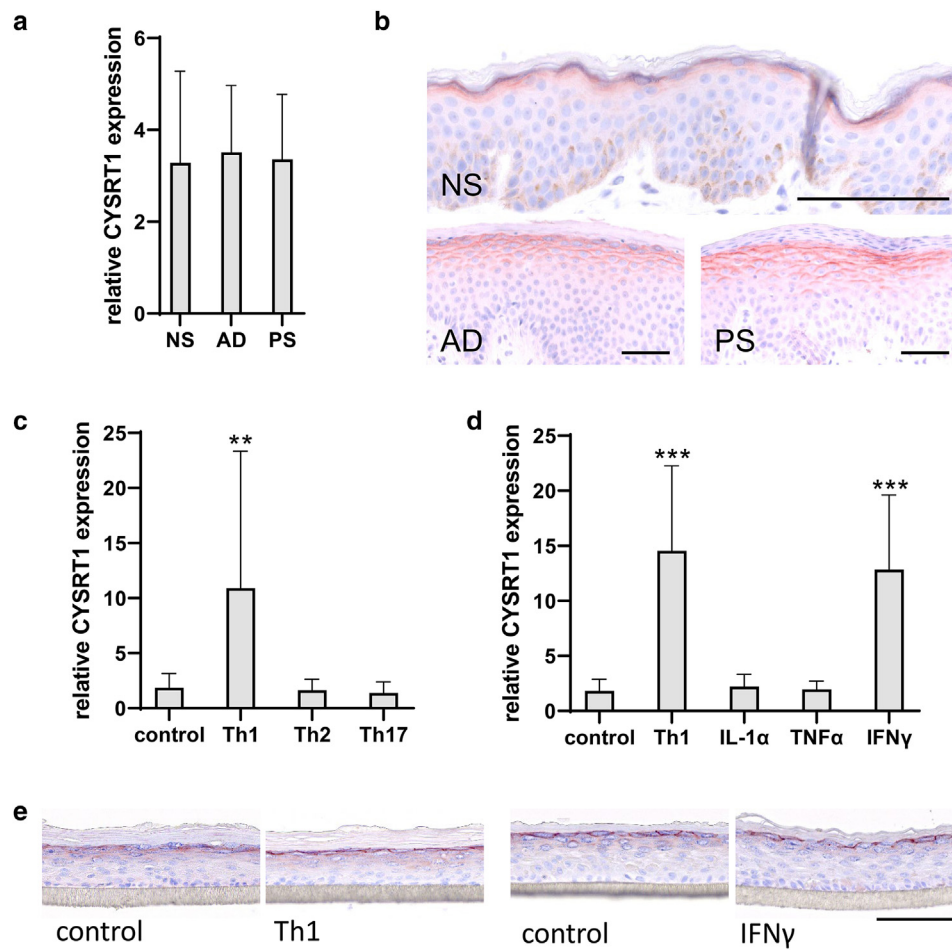


Figure 2. CYSRT1 gene and protein expression in human tissues. (a) Relative mRNA expression levels of *CYSRT1* in normal human tissues, as determined by real-time qPCR. For graphic representation, values are expressed relative to *CYSRT1* in the skin, which was set at unity, to enable comparison of expression levels between tissues. (b) Immunohistochemical protein staining of *CYSRT1* in skin and oral tissues. Bar = 100 μ m. (c) Immunofluorescence detection of *CYSRT1* (green signal), anti-LCE2 (white signal), and anti-LCE3 (red signal) in normal human skin using confocal microscopy. Nuclei are stained with DAPI (blue signal). Spatial colocalization of *CYSRT1*, LCE2, and LCE3 at the cell membrane in dying stratum granulosum cells is indicated with white arrowheads. The green arrowheads indicate *CYSRT1* staining in the stratum corneum. Bar = 10 μ m. LCE, late cornified envelope.

protein expression was barely detectable in the standard (control) cultures on day 4, whereas on that same day, acceleration of epidermal development by the effect of coal tar treatment clearly coincided with elevated *CYSRT1* levels (Figure 4h). Upon knockdown of both AHR and ARNT (the AHR nuclear translocator protein) in primary KCs, *CYSRT1*

upregulation was inhibited (Figure 4i). Furthermore, HEEs derived from N/TERT-2G KCs and treated with the pure AHR agonist TCDD (2,3,7,8-tetrachlorodibenzo-p-dioxin) and/or with GNF-351 (a selective AHR antagonist) showed AHR-dependent *CYSRT1* expression under both basal and stimulated conditions (Figure 4j).

Figure 3. CYSRT1 expression in inflammatory conditions. (a) Relative mRNA expression levels of *CYSRT1* in NS ($n = 6$), AD skin ($n = 6$), and PS ($n = 11$). (b) Immunohistochemical protein staining of *CYSRT1* in NS, AD, and PS skin. (c) Relative mRNA expression levels of *CYSRT1* in monolayer cultured keratinocytes ($n = 26$) stimulated with disease-associated cytokine mixtures, and (d) with Th1 cytokines added separately to the cultures ($n = 4$ for each group). For graphic representation, values are expressed relative to *CYSRT1* in nonstimulated samples (control). (e) *CYSRT1* protein staining in HEEs stimulated with a mixture of Th1 cytokines and IFN- γ separately. Bars indicate the mean \pm SD. ** $P < 0.01$ and *** $P < 0.001$. Bars = 100 μ m. AD, atopic dermatitis; HEE, human epidermal equivalent; NS, normal skin; PS, psoriasis skin; Th1, T helper 1.



CYSRT1 has antibacterial properties

We showed by Y2H and Co-IP analysis that CYSRT1 is an interaction partner of LCE proteins in vitro with coexpression patterns in the epidermis. Knowing that LCE proteins have antimicrobial properties, probably on the basis of their CIDAMP activity, we further looked at the 144 amino acid composition of CYSRT1. CYSRT1 appears rich in disorder-promoting polar amino acids (55.6% arginine, aspartic acid, glutamic acid, glutamine, glycine, histidine, lysine, proline, and serine) and low in order-promoting hydrophobic amino acids (18.1% isoleucine, leucine, methionine, phenylalanine, tryptophan, tyrosine, and valine) (Figure 5a and b), which qualifies CYSRT1 as a potential CIDAMP (Campen et al., 2008; Latendorf et al., 2019). We therefore hypothesized that CYSRT1 has an antimicrobial function in the epidermis. Indeed, full-length recombinant CYSRT1 exhibited antibacterial activity against *Pseudomonas aeruginosa* bacteria, as reported for other CIDAMPs (Figure 5c).

DISCUSSION

Recently, we reported that all LCE family proteins possess antimicrobial activity, with differences in killing efficiency and specificity between the LCE proteins and their target microbes. Because many proteins interact with other proteins to function properly in both health and disease, we were interested in possible interaction partners for these

LCE proteins. In this study, we identified CYSRT1, a hitherto poorly characterized protein, as a skin and oral epithelia-specific protein with an antibacterial activity that can interact with LCE proteins.

We could confirm positive in vitro CYSRT1–LCE protein interactions (Y2H and yeast 1-to-1 analyses) by Co-IP, except for LCE3B and LCE6A. For the latter, this can be explained by the fact that LCE6A is very different from the other LCE proteins at the amino acid level. One limitation of the Co-IP experiments is that the expression levels of the FLAG-tagged LCE and HA-tagged CYSRT1 proteins could not be controlled. Therefore, the variation in the total amount of protein does not allow for a comparison of the stoichiometry of binding between LCE proteins and CYSRT1. To confirm our observations, we took advantage of the very recently presented Human Reference Interactome, a systematically generated human protein interactome map with >50,000 protein–protein interactions of high biophysical quality (Luck et al., 2020). Using the Human Reference Interactome atlas as a reference (www.interactome-atlas.org), we found that CYSRT1 does indeed interact with itself, which we also observed in our yeast 1-to-1 analysis, and interactions with all LCE proteins except for LCE6A were confirmed. When LCE3A is used as a query in the Human Reference Interactome database, TGM1 emerges as an interactor. This is interesting because TGM1 catalyzes the crosslinking reaction

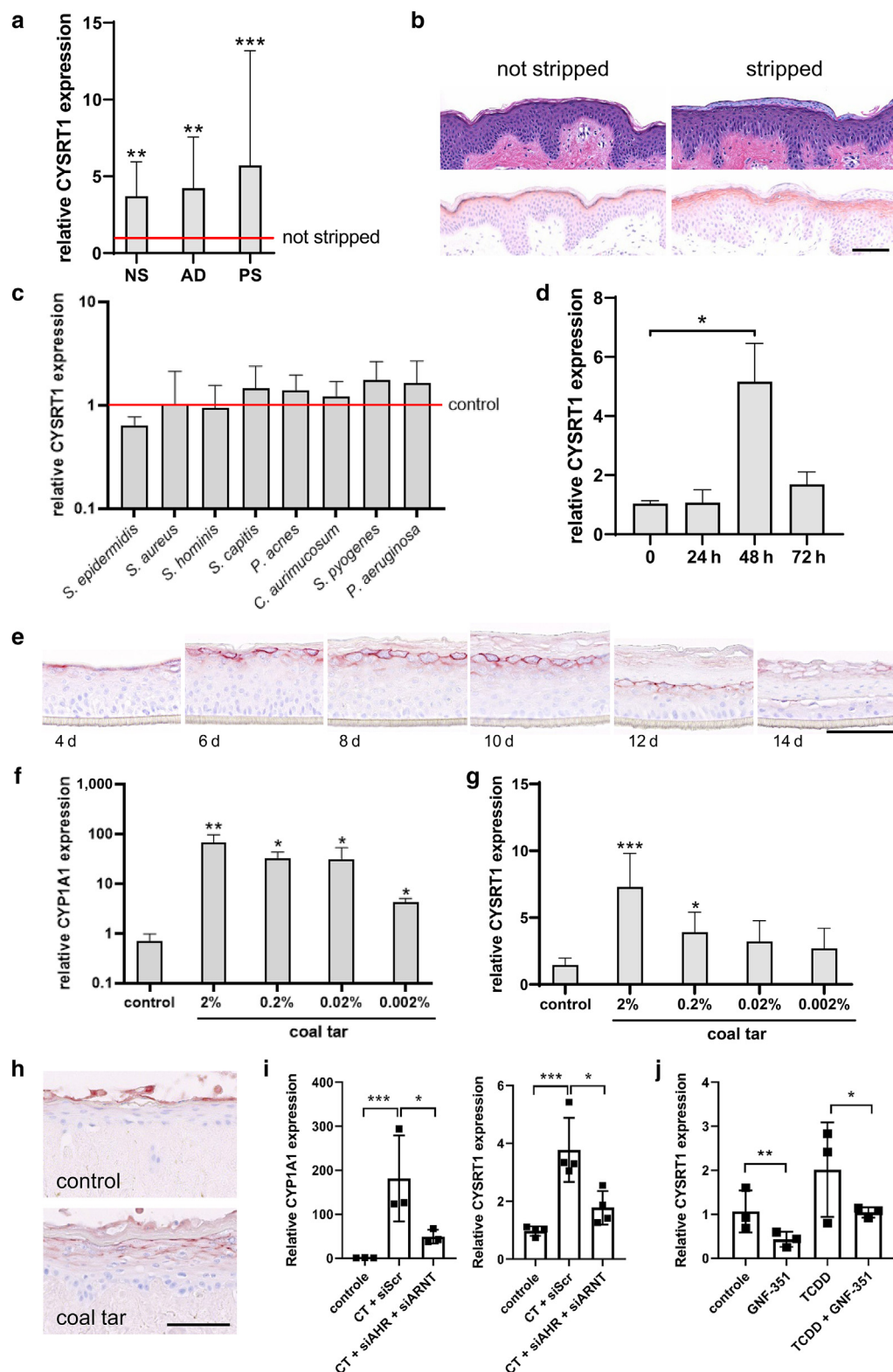


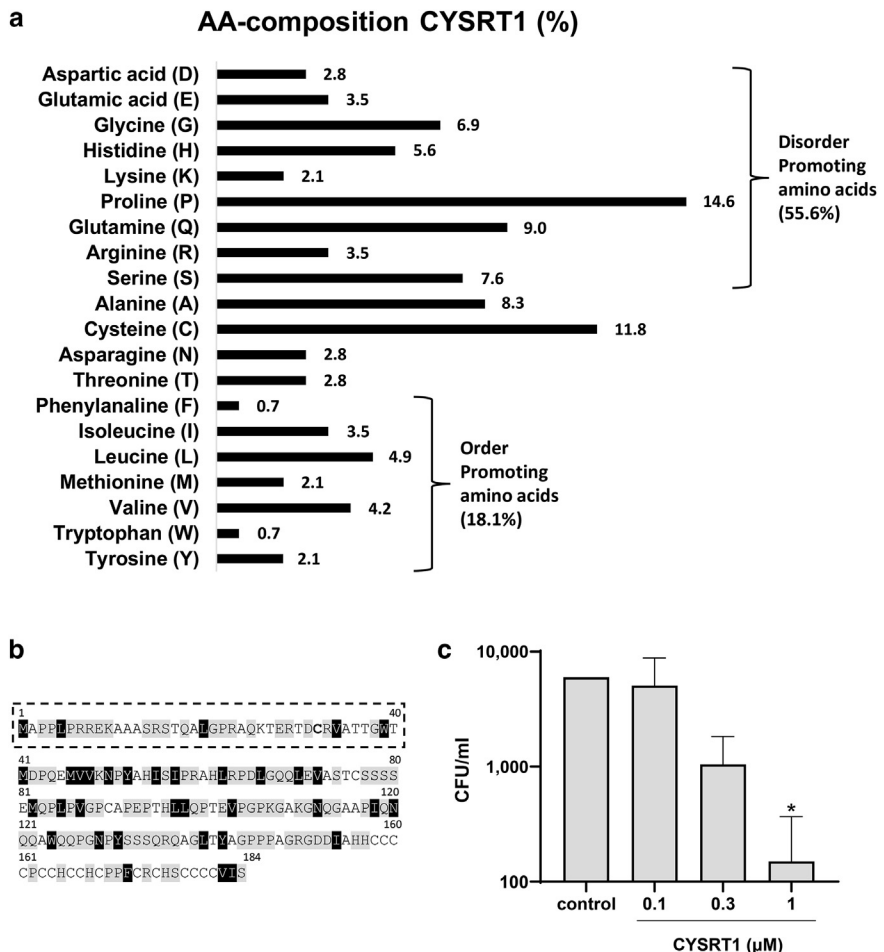
Figure 4. Barrier disruption induces CYSRT1 expression. (a) Relative epidermal CYSRT1 mRNA levels in NS ($n = 6$) and nonlesional skin from patients with AD ($n = 9$) and patients with psoriasis ($n = 11$) before and after tape stripping. Values are expressed relative to CYSRT1 values before tape stripping. (b) CYSRT1 protein levels in tape-stripped normal skin. (c) CYSRT1 mRNA levels in submerged cultured keratinocytes ($n = 5$) exposed to live bacteria. Values were expressed relative to CYSRT1 values in nonexposed cultures. (d) CYSRT1 mRNA levels studied over time in submerged keratinocytes ($n = 3$) and (e) CYSRT1 protein levels in 3D HEEs. (f) CYSRT1 and (g) CYP1A1 mRNA levels in submerged cultured keratinocytes ($n = 3$) exposed to a dilution series of coal tar for 24 hours. (h) CYSRT1 protein expression in human skin equivalents on day 4 of the air–liquid interface culture when cultured in the presence or absence (control) of coal tar. Images are representative of three keratinocyte donors, and the experiment was replicated twice. (i) CYSRT1 and CYP1A1 are induced upon coal tar treatment of submerged monolayer cultured keratinocytes, and their induction can be hampered by siRNA-mediated knockdown of AHR and its nuclear partner ARNT. (j) Inhibition of AHR signaling by GNF-351 downregulates CYSRT1 expression both under basal conditions (vs. control) and upon ligand activation (vs. TCDD). Bars indicate mean \pm SD. * $P < 0.05$, ** $P < 0.01$, and *** $P < 0.001$. Bars = 100 μ m. 3D, three-dimensional; AD, atopic dermatitis; AHR, aryl hydrocarbon receptor; d, day; h, hour; HEE, human epidermal equivalent; NS, normal skin; PS, psoriasis skin; siAHR, aryl hydrocarbon receptor–small interfering RNA; siARNT, ARNT-targeted small interfering RNA; siRNA, small interfering RNA; siScr, scramble-targeted small interfering RNA.

of epidermal proteins during the formation of the stratum corneum (Eckhart et al., 2013). We also identified TGM1 as an interaction partner for LCE3A in our Y2H screen; yet, this protein–protein interaction could not be confirmed in our yeast 1-to-1 assay (data not shown) and was therefore not further investigated. However, confocal microscopy analysis

revealed that CYSRT1, LCE2, and LCE3 are colocalized along the cell membrane of the outer granular cells of the epidermis. Whether and when they meet and possibly interact at that specific location might be explored in future research.

We observed tissue-specific expression for CYSRT1 in skin and oral epithelia, suggesting an important role for this

Figure 5. Antibacterial activity of CYSRT1 against *Pseudomonas aeruginosa*. (a) An overview of the amino acid composition of the 144 amino acids length of the CYSRT1 protein, in percentages. (b) The amino acid sequence of both CYSRT1 splice variants. The dashed box indicates the extra 40 amino acids of the long (184 amino acids) CYSRT1 variant. Amino acids highlighted in gray represent disorder-promoting polar amino acids, whereas the order-promoting hydrophobic amino acids are highlighted in black. (c) Full-length CYSRT1 was tested for antibacterial activity against *Pseudomonas aeruginosa* at increasing concentrations of 0.1, 0.3, and 1 μ M in a low salt (10 mM) buffer. Graphs show CFUs count after 2 hours before incubation, followed by overnight growth on blood agar. A total of 1×10^2 CFU/ml is the detection limit; therefore, lower values are not depicted. The assay is performed in triplicate. Bars indicate mean \pm SD. * $P < 0.05$. CFU, colony forming unit.



protein in these tissues. Indeed, expression profiling by whole-genome microarray of various normal tissues showed high expression of *CYSRT1* in skin and tonsil epithelium (Gene Expression Omnibus Accession number GDS3113) (Dezso et al., 2008). Furthermore, *CYSRT1* was found to be part of the (insoluble) cross-linked cornified envelope fraction in a human stratum corneum proteomics study (Karim et al., 2019). By confocal microscopy, we could also clearly detect the *CYSRT1* protein in the stratum corneum of skin biopsies (Figure 2c). Another indication that *CYSRT1* plays a role in the oral epithelium is its identification as a hub gene in the pathogenesis of oral squamous cell carcinoma because *CYSRT1* was found to be significantly downregulated in oral squamous cell carcinoma samples compared with that in samples derived from healthy individuals (Zhang et al., 2018). Hub genes are genes that have many interactions with others in a gene network and usually play an essential role in gene regulation and biological processes (Yu et al., 2017). In contrast to the induction of *CYSRT1* protein expression in benign inflammatory conditions such as psoriasis and atopic eczema and the increase of *CYSRT1* expression after skin barrier disruption, *CYSRT1* gene expression appears to be downregulated in skin cancer. For example, in a study using public genomic data, 368 tissue samples of metastatic melanoma of the skin were compared with 103 tissue samples from cases of primary melanoma.

Data processing identified the mRNA of *CYSRT1* as a downregulated gene in metastatic melanoma (Wang et al., 2019). The downregulation of *CYSRT1* in epithelial cancers is possibly related to the loss of differentiation of epithelial cells because, as we have also seen in our three-dimensional HEEs after prolonged culture time. Furthermore, transcriptomics by RNA sequencing on tissue samples from 95 human individuals (representing 27 different tissues) revealed a relatively high *CYSRT1* expression in the esophagus (Bio-Project number PRJEB4337) (Fagerberg et al., 2014), which we also found in our tissue panel by qPCR analysis. In addition, *CYSRT1* also appears in a coexpression network analysis that identified key modules and hub genes implicated in esophageal squamous cell cancer progression (Wang et al., 2021). However, to investigate the role and underlying molecular function of *CYSRT1* in the pathogenesis of these epithelial carcinomas, more dedicated studies are needed.

Our experiments revealed that *CYSRT1* expression is strongly induced by skin barrier disruption. From earlier work, we know that several host defense genes (AMPs) can be induced by microbes (Zeeuwen et al., 2017), including LCE3A, whose expression was provoked by *Pseudomonas aeruginosa* (our unpublished observation). However, the induced *CYSRT1* expression upon skin barrier disruption does not seem to be the result of host response mechanisms against microbes but rather relates to the terminal

differentiation status of KCs. The terminal epidermal differentiation program is tightly coordinated by a plethora of transcription factors; among these, the AHR has our special interest because it can be ligand activated and controllable by therapeutics. In the nucleus, AHR binds to specific xenobiotic response elements in the DNA (Denison et al., 1988) to control gene transcription. However, the promotor region of CYSRT1 does not contain such putative AHR-binding elements, suggesting an indirect effect of AHR activation on CYSRT1 expression. Most likely, terminal differentiation and thus CYSRT1 expression are late effects of AHR activation owing to other transcription factors important for driving epidermal differentiation that are target genes or interaction partners of AHR, such as OVOL-1 or NRF-2 (Furue, 2020).

Recently, we showed that the antimicrobial activity of LCE proteins is dependent on, among others, high content of disorder-promoting amino acids, the peptide chain length, and the cumulative effect of positively charged amino acids (Niehues et al., 2022). Similar to LCE3A, CYSRT1 is a very cationic protein (respectively, 17.4 and 16% positively charged amino acids) with a high cysteine (11.8%) and proline (14.6%) content (the percentages of cysteine and proline residues in LCE3A are 14.6 and 10.1%, respectively). Most cysteine residues are located at the C-terminus of CYSRT1. A high percentage of cysteine residues can increase stability against proteolysis, high temperature, and pH changes (González-Castro et al., 2021), which may be important for an AMP in the stratum corneum. The isoelectric point (6.67) of the 144 amino acids transcribed into the CYSRT1 protein is lower than that of LCE3A and the other LCE proteins (8.5–9.0) (Niehues et al., 2022). RNA-sequencing analysis of human KCs that we recently performed (unpublished observation) showed that the CYSRT1 transcript in KCs encodes the 144 amino acid protein splice variant (isoform), whereas both transcripts are present in the used human reference genome (i.e., hg38, with Ensembl transcript identifications ENST00000650725 and ENST00000409414 for the short and long transcripts, respectively). This contradiction with our western blot data forced us to review the amino acid sequence of CYSRT1. We searched for potential post-translational modification sites in the protein that could explain the size of 18–20 kDa (instead of the expected size of ~15 kDa). Using PhosphoSitePlus (Cell Signaling Technology, Danvers, MA; www.phosphosite.org), eight predicted phosphorylation sites were found in the 144 amino acids of the CYSRT1 protein. Because the addition of a phosphoryl group adds approximately 1 kDa to the molecular weight (in theory and depending on the protein), multiple phosphorylation sites can lead to more significant molecular weight changes. The strong 18–20 kDa band suggests that indeed post-translational modifications have occurred, although it is remarkable that only a few light bands are visible with a lower kDa. One could expect protein variants of different sizes, that is, with and without post-translational modification. Therefore, the existence of putatively two transcripts in the skin is something to consider in future research.

Finally, we found that CYSRT1 can act as an antibacterial protein and kill *Pseudomonas aeruginosa*, just as it has been

shown for other epidermal structural proteins such as hornerin, FLG2, and LCEs (Latendorf et al., 2019; Niehues et al., 2022, 2017). A remarkable structural feature of CYSRT1 is the conserved C-terminal clustering of many cysteine residues, together with pairs of histidine and some aspartic acid residues. These amino acids should be able to form binding sites for transition metals (e.g., Zn²⁺, Mn²⁺, Fe²⁺, and Cu²⁺) that are essential to various microorganisms. Several skin-derived AMPs contain such binding sites, and metal depletion has been shown as the antimicrobial mode of action (Diaz-Ochoa et al., 2014; Nelson et al., 2021), among which CYSRT1 may now be considered. It should be noted that the in vitro antimicrobial test conditions are quite different from the natural environment in which these AMPs normally operate. AMPs are typically tested at low micromolar concentrations as well as low salt concentrations, both of which can actually be multiple times higher in vivo at specific skin microenvironments. For example, we have previously shown using an in vitro reconstructed skin model that a higher concentration of endogenous human β-defensin-2 can be achieved (up to 300 mM) than is required for antibacterial activity (Jansen et al., 2009), which may compensate for the higher salinity in vivo. It was previously suggested that antimicrobial factors of the stratum corneum, such as fragments of the intrinsically disordered protein hornerin, may actively control the growth of *Pseudomonas aeruginosa* on the skin of a healthy individual (Latendorf et al., 2019). Whether CYSRT1 is also active against other cutaneous species (commensals and pathogens) and at what concentrations and environmental conditions are a topic for future research.

MATERIALS AND METHODS

Constructs

For specifications of all constructs and used gene-specific primers, see [Supplementary Materials and Methods](#).

Y2H screen and yeast 1-to-1 assays

The GAL4-based Y2H system (HybriZAP, Stratagene, La Jolla, CA) was used for the identification of protein interaction partners of LCE3A, LCE3B, and LCE3C. For details regarding these assays, see [Supplementary Materials and Methods](#).

Cell culture, transfection, and preparation of lysates for Co-IP and western blot analysis

For Co-IP experiments, human embryonic kidney 293T cells were transfected with pcDNA3-HA/DEST-CYSRT1 and p3xFLAG-CMV/DEST-LCE constructs. For further details of the cell culture, transfection procedure, and lysate preparation, see [Supplementary Materials and Methods](#).

Human tissues

Collection of archive autopsy material, taking skin biopsies from healthy volunteers and patients, and stratum corneum removal by tape stripping were performed as described before (Bergboer et al., 2011; de Koning et al., 2012, 2011). The study was conducted according to the Declaration of Helsinki principles, and research on the obtained material was performed in accordance with institutional review board approval from the local ethics committee of the Radboud University Medical Center (Nijmegen, The Netherlands). All human subjects have provided written informed consent.

RNA isolation and real-time quantitative PCR

RNA isolation, cDNA synthesis, primer design, and RT-qPCR were performed as described previously (Smits et al., 2017). *CYSRT1* gene expression (forward primer: 5'-AGAGGACAGACTGCCGTGG-3' and reverse primer: 5'-GGGTTCTGACGACCATCTCTT-3') was normalized to the expression of the housekeeping gene *RPLPO* (forward primer: 5'-CACCATGAAATCCTGAGTGATGT-3' and reverse primer: 5'-TGACCAGCCCAAAGGAGAAG-3'). The $\Delta\Delta Ct$ method was used to calculate relative mRNA expression levels (Livak and Schmittgen, 2001). Statistics were performed on ΔCt levels using a Student's *t*-test for comparing different groups and a paired *t*-test for comparing treated and untreated samples.

Bacterial stimulation of submerged cultured KCs

Primary human KCs obtained from abdominal plastic skin surgery were isolated and expanded according to the Rheinwald–Green protocol (Rheinwald and Green, 1975) and stored in liquid nitrogen. Primary human KCs or N/TERT KCs, an immortalized KC cell line purchased from J. Rheinwald Laboratory (Harvard Medical School, Boston, MA), were cultured without antibiotics as described earlier (Nygaard et al., 2015; Smits et al., 2017). For bacterial stimulations, see Supplementary Materials and Methods.

Human skin and epidermal equivalent cultures

Human skin equivalents were generated using de-epidermized dermis, as described previously, and seeded with 10^5 human primary KCs. Human skin equivalents were cultured and submerged for 3 days, after which the medium level was decreased, and equivalents were cultured for 4 days at the air–liquid interface with/without the presence of coal tar (van den Bogaard et al., 2013). The three-dimensional HEEs were cultured as described earlier (Rikken et al., 2020). The T helper 1–cytokine mixture (10 ng/ml IL-1 α , 0.5 ng/ml TNF α , and 250 U/ml IFN- γ) or IFN- γ alone (250 U/ml) (all cytokines from Preprotech, Rocky Hill, NJ) were added into the culture medium from day 5 until day 8 of the air–liquid interface and harvested on day 8 for further analysis (Niehues et al., 2021). Because of the toxicity of the cells, the concentrations of the cytokines used in three-dimensional HEEs are lower than the concentrations used to stimulate submerged cultured KCs (Niehues et al., 2021). For TCDD (10 nM; Accustandard, New Haven, CT) and GNF-351 (500 nM; Sigma, St. Louis, MO) stimulation (72 hours of stimulation before harvesting), HEEs were generated from N/TERT-2G KCs and cultured in triplicate per experimental condition.

Small interfering RNA knockdown

KCs were grown to 60% confluence, and 500 nM of smartpool (AHR-targeted small interfering RNA and ARNT-targeted small interfering RNA) or nontargeting small interfering RNA (Accell Dharmacon, Thermo Fisher Scientific, Waltham, MA) was added for 48 hours (Smits et al., 2020). The culture medium was subsequently refreshed and supplemented with small interfering RNA for another 24 hours. Thereafter, KCs were allowed to differentiate for 48 hours in the presence of 2 μ g/ml coal tar (Fagron BV, Capelle aan de IJssel, The Netherlands). Cells were harvested for transcriptional analysis.

Immunohistochemistry, immunofluorescence, and confocal microscopy

Detection of the CYSRT1 protein was performed by microscopy and described in detail in the Supplementary Materials and Methods.

Western blotting CYSRT1

Detection of endogenously expressed CYSRT1 in HEEs derived from primary human KCs was done by western blotting as described in the Supplementary Materials and Methods.

Antibacterial assay

Antibacterial assay was performed as described earlier (Niehues et al., 2022). For exact details regarding this assay, see Supplementary Materials and Methods.

Statistics

For details of the statistical analyses, see Supplementary Materials and Methods.

Data availability statement

The authors confirm that all the data supporting the findings of this study are available within the article and its supplementary materials.

ORCIDs

Hanna Niehues: <http://orcid.org/0000-0002-6954-6955>

Gijs Rikken: <http://orcid.org/0000-0003-0535-5399>

Ferry F. J. Kersten: <http://orcid.org/0000-0002-4183-6504>

Jorine Eeftens: <http://orcid.org/0000-0001-6784-9955>

Ivonne M. J. J. van Vlijmen-Willems: <http://orcid.org/0000-0002-3522-2573>

Diana Rodijk-Olthuis: <http://orcid.org/0000-0002-7752-6209>

Patrick A. M. Jansen: <http://orcid.org/0000-0002-7894-2140>

Wiljan Hendriks: <http://orcid.org/0000-0001-9481-8281>

Thomas H. A. Ederveen: <http://orcid.org/0000-0003-0068-1275>

Joost Schalkwijk: <http://orcid.org/0000-0002-1308-1319>

Ellen H. van den Bogaard: <http://orcid.org/0000-0003-4846-0287>

Patrick L. J. M. Zeeuwen: <http://orcid.org/0000-0002-6878-2438>

CONFLICT OF INTEREST

The authors state no conflict of interest.

ACKNOWLEDGMENTS

Danique A. van der Krieken, Merel A. W. Oortveld, and Felicitas Pardow are acknowledged for excellent technical assistance. Jos P. H. Smits and Noa J. M. van den Brink provided biological samples for expression analysis studies. All are affiliated with the department of Dermatology, Radboud University Nijmegen Medical Center (Radboudumc) (Nijmegen, The Netherlands). This work was supported by an ALW-grant 821.02.013 (to JS and PLJMZ) from ZonMw, the Netherlands Organization for Health Research and Development. Parts of this work were funded by the National Institutes of Health (ES028244 subaward to EHVDB).

AUTHOR CONTRIBUTION

Conceptualization: HN, JS, EHVDB, PLJMZ; Data Curation: HN, EHVDB, PLJMZ; Formal Analysis: HN, GR, FFJK, JE, PAMJ, IMJJVVW; Funding Acquisition: JS, PLJMZ; Investigation: HN, GR, FFJK, JE, IMJJVVW, DRO, PAMJ, THAE, JS, EHVDB, PLJMZ; Methodology: HN, GR, FFJK, WH, JS, EHVDB, PLJMZ; Project Administration: HN, EHVDB, PLJMZ; Resources: HN, GR, FFJK, JS, EHVDB, PLJMZ; Supervision: EHVDB, PLJMZ; Validation: HN, JS, EHVDB, PLJMZ; Visualization: HN, THAE, PLJMZ; Writing – Original Draft Preparation: HN, PLJMZ; Writing – Review and Editing: HN, WH, THAE, JS, EHVDB, PLJMZ

SUPPLEMENTARY MATERIAL

Supplementary material is linked to the online version of the paper at www.jidonline.org, and at <https://doi.org/10.1016/j.jid.2023.01.022>

REFERENCES

- Bergboer JG, Tjabringa GS, Kamsteeg M, van Vlijmen-Willems IM, Rodijk-Olthuis D, Jansen PA, et al. Psoriasis risk genes of the late cornified envelope-3 group are distinctly expressed compared with genes of other LCE groups. *Am J Pathol* 2011;178:1470–7.
- Bergboer JG, Zeeuwen PL, Schalkwijk J. Genetics of psoriasis: evidence for epistatic interaction between skin barrier abnormalities and immune deviation. *J Invest Dermatol* 2012;132:2320–31.
- Bissonnette R, Stein Gold L, Rubenstein DS, Tallman AM, Armstrong A. Tapinarof in the treatment of psoriasis: a review of the unique mechanism

- of action of a novel therapeutic aryl hydrocarbon receptor-modulating agent. *J Am Acad Dermatol* 2021;84:1059–67.
- Büchau AS, Hassan M, Kukova G, Lewerenz V, Kellermann S, Würthner JU, et al. S100A15, an antimicrobial protein of the skin: regulation by *E. coli* through toll-like receptor 4. *J Invest Dermatol* 2007;127:2596–604.
- Campen A, Williams RM, Brown CJ, Meng J, Uversky VN, Dunker AK. TOP-IDP-scale: a new amino acid scale measuring propensity for intrinsic disorder. *Protein Pept Lett* 2008;15:956–63.
- Chang HW, Yan D, Singh R, Liu J, Lu X, Ucmak D, et al. Alteration of the cutaneous microbiome in psoriasis and potential role in Th17 polarization. *Microbiome* 2018;6:154.
- de Cid R, Riveira-Munoz E, Zeeuwen PL, Robarge J, Liao W, Danhauer EN, et al. Deletion of the late cornified envelope LCE3B and LCE3C genes as a susceptibility factor for psoriasis. *Nat Genet* 2009;41:211–5.
- de Koning HD, Kamsteeg M, Rodijk-Olthuis D, van Vlijmen-Willems IM, van Erp PE, Schalkwijk J, et al. Epidermal expression of host response genes upon skin barrier disruption in normal skin and uninvolved skin of psoriasis and atopic dermatitis patients. *J Invest Dermatol* 2011;131:263–6.
- de Koning HD, van den Bogaard EH, Bergboer JG, Kamsteeg M, van Vlijmen-Willems IM, Hitomi K, et al. Expression profile of cornified envelope structural proteins and keratinocyte differentiation-regulating proteins during skin barrier repair. *Br J Dermatol* 2012;166:1245–54.
- Denison MS, Fisher JM, Whitlock JP Jr. Inducible, receptor-dependent protein-DNA interactions at a dioxin-responsive transcriptional enhancer. *Proc Natl Acad Sci USA* 1988;85:2528–32.
- Dezso Z, Nikolsky Y, Sviridov E, Shi W, Serebriyskaya T, Dosymbekov D, et al. A comprehensive functional analysis of tissue specificity of human gene expression. *BMC Biol* 2008;6:49.
- Diaz-Ochoa VE, Jellbauer S, Klaus S, Raffatelli M. Transition metal ions at the crossroads of mucosal immunity and microbial pathogenesis. *Front Cell Infect Microbiol* 2014;4:2.
- Eckhart L, Lippens S, Tschachler E, Declercq W. Cell death by cornification. *Biochim Biophys Acta* 2013;1833:3471–80.
- Fagerberg L, Hallström BM, Oksvold P, Kampf C, Djureinovic D, Odeberg J, et al. Analysis of the human tissue-specific expression by genome-wide integration of transcriptomics and antibody-based proteomics. *Mol Cell Proteomics* 2014;13:397–406.
- Frohm M, Agerberth B, Ahangari G, Stähle-Bäckdahl M, Lidén S, Wigzell H, et al. The expression of the gene coding for the antibacterial peptide LL-37 is induced in human keratinocytes during inflammatory disorders. *J Biol Chem* 1997;272:15258–63.
- Furue M. Regulation of filaggrin, loricrin, and involucrin by IL-4, IL-13, IL-17A, IL-22, AHR, and NRF2: pathogenic implications in atopic dermatitis. *Int J Mol Sci* 2020;21:5382.
- Fyhrquist N, Muirhead G, Prast-Nielsen S, Jeanmougin M, Olah P, Skoog T, et al. Microbe-host interplay in atopic dermatitis and psoriasis. *Nat Commun* 2019;10:4703.
- Gerstel U, Latendorf T, Bartels J, Becker A, Tholey A, Schröder JM. Hornerin contains a Linked Series of Ribosome-Targeting Peptide antibiotics. *Sci Rep* 2018;8:16158.
- Gläser R, Harder J, Lange H, Bartels J, Christophers E, Schröder JM. Antimicrobial psoriasin (S100A7) protects human skin from *Escherichia coli* infection. *Nat Immunol* 2005;6:57–64.
- González-Castro R, Gómez-Lim MA, Plisson F. Cysteine-rich peptides: hyperstable scaffolds for protein engineering. *ChemBioChem* 2021;22: 961–73.
- Hansmann B, Schröder JM, Gerstel U. Skin-derived C-terminal filaggrin-2 fragments are *Pseudomonas aeruginosa*-directed antimicrobials targeting bacterial replication. *PLOS Pathog* 2015;11:e1005159.
- Harder J, Bartels J, Christophers E, Schröder JM. A peptide antibiotic from human skin. *Nature* 1997;387:861.
- Hiemstra PS, Maassen RJ, Stolk J, Heinzel-Wieland R, Steffens GJ, Dijkman JH. Antibacterial activity of antileukoprotease. *Infect Immun* 1996;64:4520–4.
- Hollox EJ, Huffmeier U, Zeeuwen PL, Palla R, Lascorz J, Rodijk-Olthuis D, et al. Psoriasis is associated with increased beta-defensin genomic copy number. *Nat Genet* 2008;40:23–5.
- Huffmeier U, Bergboer JG, Becker T, Armour JA, Traupe H, Estivill X, et al. Replication of LCE3C-LCE3B CNV as a risk factor for psoriasis and analysis of interaction with other genetic risk factors. *J Invest Dermatol* 2010;130: 979–84.
- Jansen PA, Rodijk-Olthuis D, Hollox EJ, Kamsteeg M, Tjabringa GS, de Jongh GJ, et al. Beta-defensin-2 protein is a serum biomarker for disease activity in psoriasis and reaches biologically relevant concentrations in lesional skin. *PLoS One* 2009;4:e4725.
- Karim N, Phinney BS, Salemi M, Wu PW, Naeem M, Rice RH. Human stratum corneum proteomics reveals cross-linking of a broad spectrum of proteins in cornified envelopes. *Exp Dermatol* 2019;28:618–22.
- Kong HH, Oh J, Deming C, Conlan S, Grice EA, Beatson MA, et al. Temporal shifts in the skin microbiome associated with disease flares and treatment in children with atopic dermatitis. *Genome Res* 2012;22:850–9.
- Latendorf T, Gerstel U, Wu Z, Bartels J, Becker A, Tholey A, et al. Cationic intrinsically disordered antimicrobial peptides (CIDAMPs) represent a new paradigm of innate defense with a potential for novel anti-infectives. *Sci Rep* 2019;9:3331.
- Liu L, Wang L, Jia HP, Zhao C, Heng HH, Schutte BC, et al. Structure and mapping of the human beta-defensin HBD-2 gene and its expression at sites of inflammation. *Gene* 1998;222:237–44.
- Livak KJ, Schmittgen TD. Analysis of relative gene expression data using real-time quantitative PCR and the 2(-Delta Delta C(T)) Method. *Methods* 2001;25:402–8.
- Luck K, Kim DK, Lambourne L, Spirohn K, Begg BE, Bian W, et al. A reference map of the human binary protein interactome. *Nature* 2020;580:402–8.
- Marchini G, Lindow S, Brismar H, Ståbi B, Berggren V, Ulfgren AK, et al. The newborn infant is protected by an innate antimicrobial barrier: peptide antibiotics are present in the skin and vernix caseosa. *Br J Dermatol* 2002;147:1127–34.
- Nelson CE, Huang W, Zygiel EM, Nolan EM, Kane MA, Oglesby AG. The human innate immune protein calprotectin elicits a multimetal starvation response in *Pseudomonas aeruginosa*. *Microbiol Spectr* 2021;9: e0051921.
- Niehues H, Rikken G, van Vlijmen-Willems IM, Rodijk-Olthuis D, van Erp PE, Zeeuwen PL, et al. Identification of keratinocyte mitogens: implications for hyperproliferation in psoriasis and atopic dermatitis. *JID Innov* 2021;2: 100066.
- Niehues H, van der Krieken DA, Ederveen THA, Jansen PAM, van Niftrik L, Mesman R, et al. Antimicrobial late cornified envelope proteins: the psoriasis risk factor deletion of LCE3B/C genes affects microbiota composition. *J Invest Dermatol* 2022;142:1947–55.e6.
- Niehues H, Tsui LC, van der Krieken DA, Jansen PA, Oortveld MA, Rodijk-Olthuis D, et al. Psoriasis-associated late cornified envelope (LCE) proteins have antibacterial activity. *J Invest Dermatol* 2017;137:2380–8.
- Niehues H, van Vlijmen-Willems IM, Bergboer JG, Kersten FF, Narita M, Hendriks WJ, et al. Late cornified envelope (LCE) proteins: distinct expression patterns of LCE2 and LCE3 members suggest nonredundant roles in human epidermis and other epithelia. *Br J Dermatol* 2016;174: 795–802.
- Nygaard UH, Niehues H, Rikken G, Rodijk-Olthuis D, Schalkwijk J, van den Bogaard EH. Antibiotics in cell culture: friend or foe? Suppression of keratinocyte growth and differentiation in monolayer cultures and 3D skin models. *Exp Dermatol* 2015;24:964–5.
- Palmer CN, Irvine AD, Terron-Kwiatkowski A, Zhao Y, Liao H, Lee SP, et al. Common loss-of-function variants of the epidermal barrier protein filaggrin are a major predisposing factor for atopic dermatitis. *Nat Genet* 2006;38: 441–6.
- Rheinwald JG, Green H. Formation of a keratinizing epithelium in culture by a cloned cell line derived from a teratoma. *Cell* 1975;6:317–30.
- Rikken G, Niehues H, van den Bogaard EH. Organotypic 3D skin models: human epidermal equivalent cultures from primary keratinocytes and immortalized keratinocyte cell lines. *Methods Mol Biol* 2020;2154: 45–61.
- Sallenave JM, Marsden MD, Ryle AP. Isolation of elafin and elastase-specific inhibitor (ESI) from bronchial secretions. Evidence of sequence homology and immunological cross-reactivity. *Biol Chem Hoppe Seyler* 1992;373: 27–33.
- Schittek B, Hipfel R, Sauer B, Bauer J, Kalbacher H, Stevanovic S, et al. Dermcidin: a novel human antibiotic peptide secreted by sweat glands. *Nat Immunol* 2001;2:1133–7.

- Smith FJ, Irvine AD, Terron-Kwiatkowski A, Sandilands A, Campbell LE, Zhao Y, et al. Loss-of-function mutations in the gene encoding filaggrin cause ichthyosis vulgaris. *Nat Genet* 2006;38:337–42.
- Smith SH, Jayawickreme C, Rickard DJ, Nicodeme E, Bui T, Simmons C, et al. Tapinarof is a natural AhR agonist that resolves skin inflammation in mice and humans. *J Invest Dermatol* 2017;137:2110–9.
- Smits JPH, Niehues H, Rikken G, van Vlijmen-Willems IMJJ, van de Zande GWJF, Zeeuwen PLJM, et al. Immortalized N/TERT keratinocytes as an alternative cell source in 3D human epidermal models. *Sci Rep* 2017;7:11838.
- van den Bogaard EH, Bergboer JG, Vonk-Bergers M, van Vlijmen-Willems IM, Hato SV, van der Valk PG, et al. Coal tar induces AhR-dependent skin barrier repair in atopic dermatitis. *J Clin Invest* 2013;123:917–27.
- van den Bogaard EH, Esser C, Perdew GH. The aryl hydrocarbon receptor at the forefront of host-microbe interactions in the skin: A perspective on current knowledge gaps and directions for future research and therapeutic applications. *Exp Dermatol* 2021;30:1477–83.
- van den Bogaard EH, Podolsky MA, Smits JP, Cui X, John C, Gowda K, et al. Genetic and pharmacological analysis identifies a physiological role for the AhR in epidermal differentiation. *J Invest Dermatol* 2015;135:1320–8.
- Smits JP, Ederveen TH, Rikken G, van den Brink NJ, van Vlijmen-Willems IM, Boekhorst J, et al. Targeting the cutaneous microbiota in atopic dermatitis by coal tar via AhR-dependent induction of antimicrobial peptides. *J Invest Dermatol* 2020;140:415–24.e10.
- Wang G, Guo S, Zhang W, Li D, Wang Y, Zhan Q. Co-expression network analysis identifies key modules and hub genes implicated in esophageal squamous cell cancer progression. *Med Omics* 2021;1:1–16.
- Wang LX, Wan C, Dong ZB, Wang BH, Liu HY, Li Y. Integrative analysis of long noncoding RNA (lncRNA), microRNA (miRNA) and mRNA expression and construction of a competing endogenous RNA (ceRNA) network in metastatic melanoma. *Med Sci Monit* 2019;25:2896–907.
- Yu D, Lim J, Wang X, Liang F, Xiao G. Enhanced construction of gene regulatory networks using hub gene information. *BMC Bioinformatics* 2017;18:186.
- Zeeuwen PL, Ederveen TH, van der Krieken DA, Niehues H, Boekhorst J, Kezic S, et al. Gram-positive anaerobe cocci are underrepresented in the microbiome of filaggrin-deficient human skin. *J Allergy Clin Immunol* 2017;139:1368–71.
- Zhang X, Feng H, Li Z, Li D, Liu S, Huang H, et al. Application of weighted gene co-expression network analysis to identify key modules and hub genes in oral squamous cell carcinoma tumorigenesis. *Oncotargets Ther* 2018;11:6001–21.



This work is licensed under a Creative Commons Attribution 4.0 International License. To view a copy of this license, visit <http://creativecommons.org/licenses/by/4.0/>

SUPPLEMENTARY MATERIALS AND METHODS

Constructs

All constructs for protein expression were generated with commercial cloning technology (Gateway, Thermo Fisher Scientific, Waltham, MA) according to the manufacturer's instructions. Cloned plasmids were transformed into TOP10 cells (Thermo Fisher Scientific). Gene-specific primers that were used to make these constructs are listed in *Supplementary Table S2*. After transformation, plasmid DNA was isolated (Miniprep kit, Sigma-Aldrich, St. Louis, MO), and the correct insertion of the constructs was checked by restriction analysis and Sanger sequencing. A list of used vectors can be found in *Supplementary Table S3*.

Yeast two-hybrid screen and yeast 1-to-1 assays

Full-length LCE3A/B/C constructs fused to a GAL4 DNA-binding domain were used as bait to screen an Oligo-dT primed human epidermis library. This library was constructed with pooled epidermal RNA from normal skin and lesional psoriatic skin biopsies. Constructs designed for yeast two-hybrid analysis were transformed in yeast using a PEG/LiAc-based method (Yeastmaker, Clontech, Palo Alto, CA) as described earlier (Letteboer and Roepman, 2008). pAD prey constructs containing the human epidermis library were transformed into the *PJ69-4α* yeast strain, whereas pBD bait constructs (containing the late cornified envelope [LCE] genes) were transformed into the *PJ69-4A* strain. Both strains carry four reporter genes: *HIS3* (histidine), *ADE2* (adenine), *MEL1* (α -galactosidase), and *LacZ* (β -galactosidase). Bait-prey interactions were analyzed by assessment of reporter gene activation on the basis of growth on selective media, α -galactosidase colorimetric plate assays (*MEL1*), and β -galactosidase colorimetric filter lift assays (*LacZ*). Positive clones were amplified by PCR with pAD-specific primers and sequenced according to the manufacturer's instructions. The obtained sequences were used to identify protein–protein interactions. Only cDNA that was in frame and in the translated region was further considered. For yeast 1-to-1 assays, identified interaction partners were cloned in both pAD and pBD vectors. After mating, interactions were analyzed by assessment of reporter gene activation on selective media and colorimetric plate assays, similar to that of the yeast two-hybrid. Interactions were only further considered if growth was observed in both situations (partner A in pAD, partner B in pBD, and vice versa).

Cell culture, transfection, and preparation of lysates

Human embryonic kidney 293T cells were grown in DMEM + GlutaMAX (Thermo Fisher Scientific, Waltham, MA) supplemented with 10% bovine calf serum, 1 mM sodium pyruvate, penicillin, and streptomycin (500 IU/l) in 75 cm² culture flasks at 37 °C in a 5% carbon dioxide atmosphere. The medium was changed every 3–4 days. Cells were grown in six-well plates and transfected at 50–60% confluence with 2 µg DNA using polyethyleneimine. After 24–48 hours, cells were lysed with lysis buffer (50 mM Tris-hydrogen chloride, pH 7.5, 150 mM sodium chloride, 0.5% Triton-X-100). A clear cell extract was obtained by centrifugation (13,000 r.p.m., 5 minutes, 4 °C).

Coimmunoprecipitation and western blot analysis

For coimmunoprecipitation experiments, human embryonic kidney 293T cells were transfected with pcDNA3-HA/DEST-CYSRT1 and p3xFLAG-CMV/DEST-LCE constructs using polyethyleneimine, as described earlier. Clear cell lysates were incubated with agarose-conjugated goat anti-HA Antibody Agarose (Sanbio BV, Uden, The Netherlands) overnight at 4 °C while shaking. Beads with bound proteins were washed five times with lysis buffer and boiled in sample buffer with dithiothreitol, after which immunocomplexes were resolved by SDS-PAGE. For western blot analysis, proteins were transferred onto polyvinylidene fluoride membranes, which were blocked, incubated with primary and secondary antibodies in Blotto blocking buffer (Thermo Fisher Scientific), and washed with Tris-buffered saline with 0.1% Tween 20. Monoclonal mouse anti-FLAG and monoclonal mouse anti-HA antibodies were diluted at 1:1,000 (Sigma-Aldrich). The secondary anti-mouse IgG horseradish peroxidase-linked antibody was diluted to 1:2,000 (Cell Signaling Technology, Danvers, MA). Bands were visualized with a chemiluminescence substrate (20X LumiGLO, Cell Signaling Technology, Danvers, MA) and Chemidoc apparatus.

Bacterial stimulation of submerged cultured keratinocytes

Pseudomonas aeruginosa (27853, ATCC, Manassas, VA), *Cutibacterium acnes* (6919, ATCC), *Streptococcus pyogenes* (12344), *Staphylococcus epidermidis* (12228, ATCC), *S. aureus* (29213, ATCC), *S. hominis*, *S. capitis* and *Corynebacterium aurimucosum* bacteria (all clinical isolates) were grown on Columbia agar with 5% sheep blood (Becton, Dickinson, Franklin Lakes, NJ) overnight (or for 2 or 4 days in case of *C. acnes*) at 37 °C as described earlier (Zeeuwen et al., 2017). From this plate, one colony was transferred to brain heart infusion medium (Mediaproducts BV, Groningen, The Netherlands) and incubated overnight at 37 °C. *C. acnes* bacteria were cultured under strictly anaerobic conditions. Bacteria were collected by centrifugation, washed twice with PBS, and finally resuspended in PBS, resulting in bacterial concentrations of 10⁷ colony-forming units (CFUs)/ml. To determine the bacterial inoculum for keratinocyte (KC) co-cultures, bacterial suspensions were serially diluted in five steps. A total of 10 µl of each dilution was placed on sheep blood agar plates and incubated overnight at 37 °C in aerobic (and anaerobic for *C. acnes*) conditions, respectively. Visible colonies on the plate were counted for each dilution. The number of CFUs was calculated: counted CFUs × dilution factor. Confluent submerged KC cultures (n = 5) were inoculated with 3.5 × 10⁵ live bacteria and incubated for 10 hours. Cells were washed after 6 hours and incubated for another 4 hours in a fresh cell culture medium before the KCs were collected (t = 10 hours). Afterward, the bacteria were washed away, and the KCs were harvested and processed for RNA isolation and real-time qPCR analysis.

Cytokine and coal tar stimulation of submerged cultured KCs

KCs were grown until confluence, whereafter coal tar (in a concentration series [van den Bogaard et al., 2013]) or cytokines were added. After 24 hours (coal tar) or 48 hours (cytokines), the KCs were harvested and processed for RNA isolation and qPCR analysis. The T helper 1–cytokine

mixture contains 30 ng/ml IL-1 α , 30 ng/ml TNF α , and 500 U/ml IFN- γ ; the T helper 2 mixture contains IL-4 and IL-13 (each 50 ng/ml); and the T helper 17–cytokine mixture contains IL-17A and IL-22 (each 30 ng/ml). All proteins are from PeproTech (London, United Kingdom).

Immunohistochemistry, immunofluorescence, and confocal microscopy

Human epidermal equivalents and tissue biopsies were fixed in a 4% buffered formalin solution, processed, and embedded in paraffin. The 6- μ m sections were stained with H&E or processed for immunohistochemistry. For immunohistochemistry, anti-CYSRT1 antibody (1:200, Santa Cruz, Heidelberg, Germany) was used with an indirect immunoperoxidase technique with avidin–biotin complex (Vectastain, Vector Laboratories, Burlingame, United Kingdom) enhancement according to the manufacturer's instructions. Hematoxylin (Sigma-Aldrich) was used to counterstain cell nuclei.

For immunofluorescence and confocal microscopy, primary antibodies were used in 1% BSA/PBS; 1:100 for CYSRT1; 1:1,000 for LCE2 (antibody provided by M. Narita, Cambridge Cancer Centre, Cambridge, United Kingdom); and 1:2,000 for LCE3 (generated by our group [Niehues et al., 2016]). As secondary antibodies, a donkey anti-goat Alexa Fluor 647 was used for anti-CYSRT1, a donkey anti-rabbit Alexa Fluor 568 was used for anti-LCE2, and a donkey anti-mouse Alexa Fluor 488 was used for anti-LCE3. All secondary antibodies (Molecular Probes, Eugene, OR) were diluted 1:200 in 1% BSA/PBS. Nuclei were counterstained with DAPI (Dako, Heverlee, Belgium). Image acquisition of immunofluorescence-stained tissue sections was performed by a ZEISS Axio Imager equipped with a ZEISS Axiocam 105 Color Digital Camera (Zeiss, Oberkochen, Germany). The ZEISS Axiocam 105 color is a compact five-megapixel camera (2,560 \times 1,920 pixels) for high-resolution images with a 1/2.5" sensor. For confocal microscopy, the Zeiss LSM900 confocal laser scanning microscope objective 63 \times numerical aperture 1.4, focal plane 1 μ m, was used. Images were chosen as representative of the whole culture or biopsies and stored in CZI format.

Western blotting endogenously expressed CYSRT1

Primary KCs from a human organotypic epidermal equivalent (human epidermal equivalent) culture were lysed (in 10 mM Tris [pH 7.8], 5 mM EDTA, 50 mM sodium chloride, 1% NP-40, 1 mM sodium orthovanadate, 1 mM phenylmethylsulphonyl fluoride, and 1 \times Roche protease inhibitor cocktail), and the lysate was centrifuged at maximum speed for 10 minutes at 4 °C to remove insoluble proteins. Before immunoblotting, lysate supernatant was separated by SDS-PAGE on a 12% Bis-Tris-gel (with/without dithiothreitol and detergents) and transferred to polyvinylidene fluoride membranes using the NuPAGE system (Life Technologies, Santa Cruz, CA). The blot was incubated overnight at 4 °C with goat anti-CYSRT antibody (1:2,000) in 5% BSA in Tris-buffered saline with 0.1% Tween 20, followed by an incubation of 60 minutes at room temperature with anti-goat IgG-biotinylated antibody (1:1,000, Vectastain). Blot was intensively washed with Tris-buffered saline with 0.1% Tween 20 and then incubated for 60 minutes at room temperature with anti-biotin horseradish peroxidase-linked antibody (Cell

Signaling Technology). After the next wash step (five times, 10 minutes), the bands on the blot were visualized with the SuperSignal West Femto Maximum Sensitivity Substrate (Thermo Fisher Scientific) and the Bio-Rad Universal Hood Gel Imager (Bio-Rad Laboratories, Hercules, CA).

Antibacterial assay

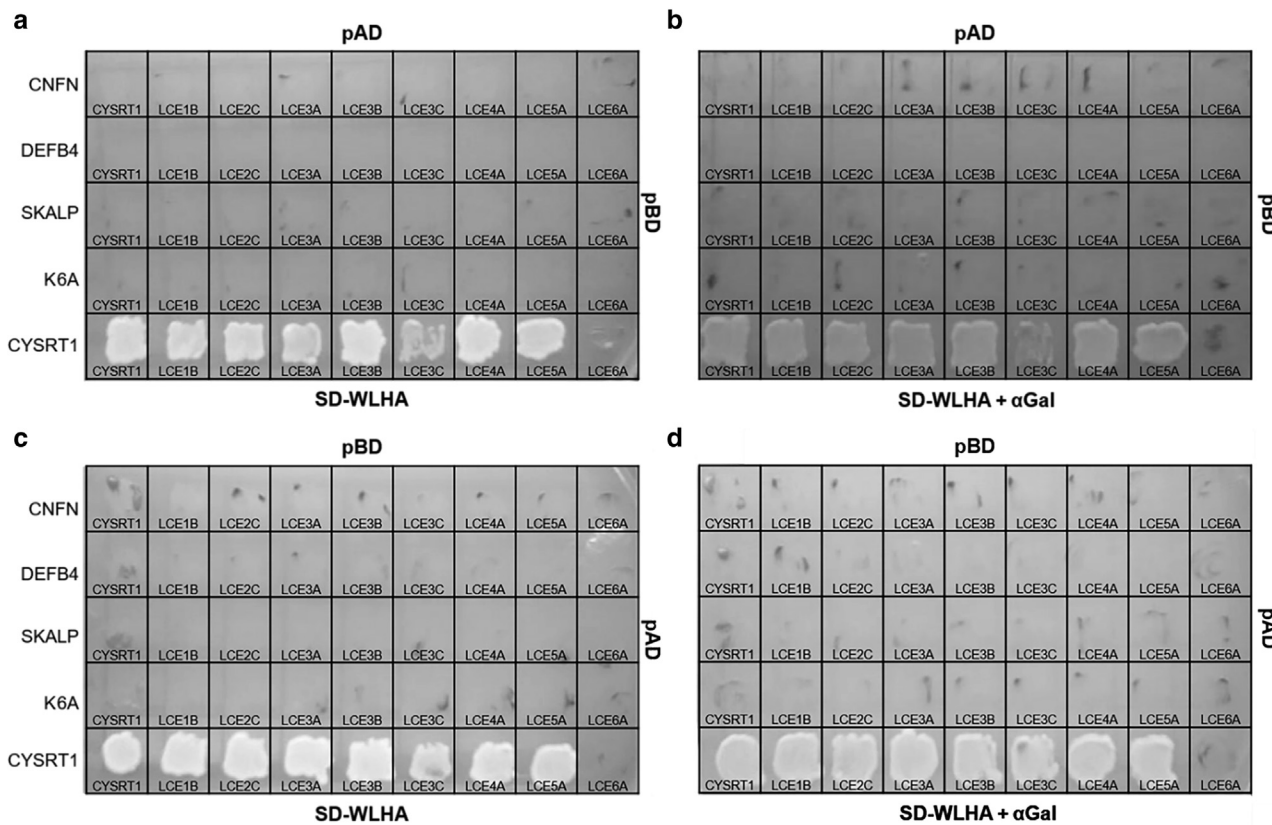
P. aeruginosa bacteria (15692, ATCC) were grown on Columbia agar with 5% sheep blood (Becton, Dickinson). From this plate, one colony was transferred to brain heart infusion medium (Mediaproducts BV) and incubated overnight at 37 °C. The next day, the bacterial suspensions were diluted 100 times in brain heart infusion and incubated for another 2.5 hours to achieve exponential growth of the bacteria. The bacteria were then harvested by centrifugation (2,100g, 5 minutes) and resuspended in low salt sodium phosphate buffer (10 mM, pH 5.5) at a concentration of 10³–10⁴ CFUs/ml. Bacterial suspensions were exposed to recombinant full-length CYSRT1 (Cusabio Biotech, Wuhan, China) for 2 hours at 37 °C. The recombinant protein was delivered lyophilized in a manufacturer's buffer (100 mM Tris-hydrogen chloride, 0.4 M Arg, pH 8.0, 10% glycerol). We dialyzed the protein to 1 mM dithiothreitol in PBS needed for experiments to omit any interaction by impurities. After the preincubation period, the CYSRT1-treated suspensions were serially diluted in PBS, plated on Columbia agar with 5% sheep blood, and incubated overnight at 37 °C. The antimicrobial effect of CYSRT1 was determined by CFU counting.

Statistics

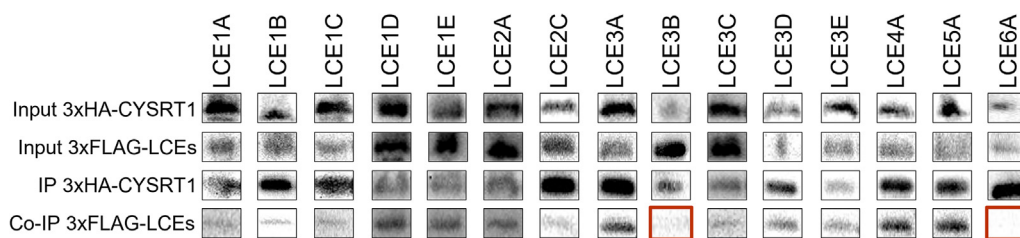
For the CFU count data of the antimicrobial assays, statistical analysis was performed using nonparametric one-sided Man–Whitney *U* test by comparing different dosages of CYSRT1 protein with those of its control. Statistical analysis of real-time qPCR gene expression data was performed on dCt values. One-way ANOVA analysis followed by Dunnett's posthoc analysis was performed for all in vitro experiments if ≥ 3 groups for comparison. *P*-values are shown with an asterisk (**P* < 0.05, ***P* < 0.01, or ****P* < 0.001) and represent significant differences in specific tested conditions compared with the control group (or specified with a bar). For the in vivo tape-stripping experiment, statistical analysis was performed with a one-tailed, pairwise Student's *t*-test comparing gene expression before and after tape stripping within each group (normal skin, atopic dermatitis skin, psoriasis skin). *P*-values are shown with an asterisk (**P* < 0.05, ***P* < 0.01, or ****P* < 0.001).

SUPPLEMENTARY REFERENCES

- Letteboer SJ, Roepman R. Versatile screening for binary protein-protein interactions by yeast two-hybrid mating. *Methods Mol Biol* 2008;484: 145–59.
- Niehues H, van Vlijmen-Willems IM, Bergboer JG, Kersten FF, Narita M, Hendriks WJ, et al. Late cornified envelope (LCE) proteins: distinct expression patterns of LCE2 and LCE3 members suggest nonredundant roles in human epidermis and other epithelia. *Br J Dermatol* 2016;174:795–802.
- van den Bogaard EH, Bergboer JG, Vonk-Bergers M, van Vlijmen-Willems IM, Hato SV, van der Valk PG, et al. Coal tar induces AHR-dependent skin barrier repair in atopic dermatitis. *J Clin Invest* 2013;123:917–27.
- Zeeuwen PL, Ederveen TH, van der Krieken DA, Niehues H, Boekhorst J, Kezic S, et al. Gram-positive anaerobe cocci are underrepresented in the microbiome of filaggrin-deficient human skin. *J Allergy Clin Immunol* 2017;139:1368–71.



Supplementary Figure S1. Yeast 1-to-1 assay. CYSRT1 and interaction partners were fused with the GAL4-AD or GAL4-BD domains (as indicated) and were then transformed into yeast cells and grown on SD-WLHA selective medium without tryptophan (W), leucine (L), histidine (H), or adenine (A). Colonies indicate an interaction of CYSRT1 with itself and all LCE proteins except with LCE6A, and a weak interaction was found for LCE3C. (a) SD-WLHA plate; LCE proteins in pAD vector. (b) SD-WLHA + α Gal plate; LCE proteins in pAD vector. (c) SD-WLHA plate; LCE proteins in pBD vector. (d) SD-WLHA + α Gal plate; LCE proteins in pBD vector. α Gal, alpha-galactosidase; LCE, late cornified envelope; SD-WLHA, SD minimal medium lacking Trp, Leu, His, and Ade.

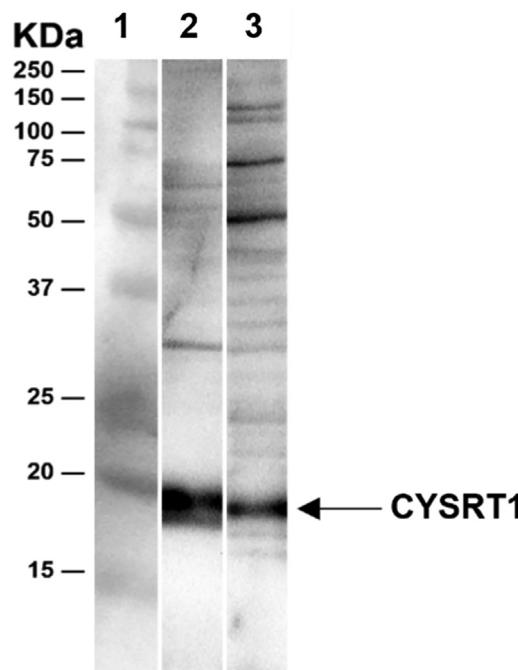


Supplementary Figure S2. Western blot of coimmunoprecipitation CYSRT1 and LCE proteins. CYSRT1 interacts with all tested LCE proteins except with LCE3B (faint signal) and LCE6A (both outlined in red). The two top panels (input) show the presence of HA-tagged CYSRT1 and FLAG-tagged LCE proteins. IP detects HA-CYSRT1 bound to the beads, and Co-IP detects the FLAG LCE protein bound to HA-CYSRT1. Note: the data (bands) in this figure are composite and taken from different western blots. Co-IP, coimmunoprecipitation; IP, immunoprecipitation; LCE, late cornified envelope.

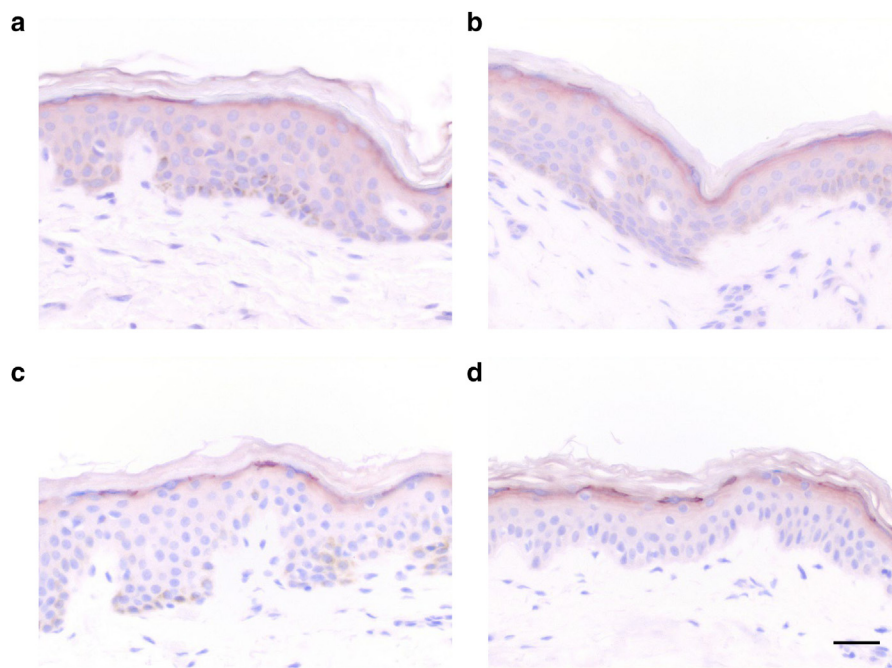
Supplementary Figure S3. *CYSR1* gene phylogenetic tree with protein alignment. This phylogenetic tree for the *CYSR1* gene is built with data that have been retrieved from the Ensembl database (gene ID ENSG00000197191; <https://www.ensembl.org>) and consists of 78

CYSRT1 orthologues genes. Ensembl lists 81 genes for *CYSRT1* in total, but we excluded the orthologues of the two nonvertebrate outgroup species *Ciona intestinalis* and *C. savignyi*, and we excluded one of the two paralogues of *Rhinopithecus bieti* because their protein products are identical (notably, it is the only species with two copies of the *CYSRT1* gene in one genome). The default comparative genomics bioinformatics workflow by Ensembl for generating the alignment data used for the creation of this figure is described on their website (<https://www.ensembl.org/info/genome/compara/index.html>). In short, the *CYSRT1* CDS back-translated protein alignment (i.e., codon alignment) is used to build five different trees (within TreeBeST; <https://github.com/Ensembl/TreeBeST>), which are thereafter merged into one consensus tree. Using this Ensembl data, the current figure of the *CYSRT1* gene phylogenetic tree with protein alignment as shown in this image has been visually recreated and customized using the iTOL tool (<https://itol.embl.de/>). CDS, CoDing Sequence; ID, identification.

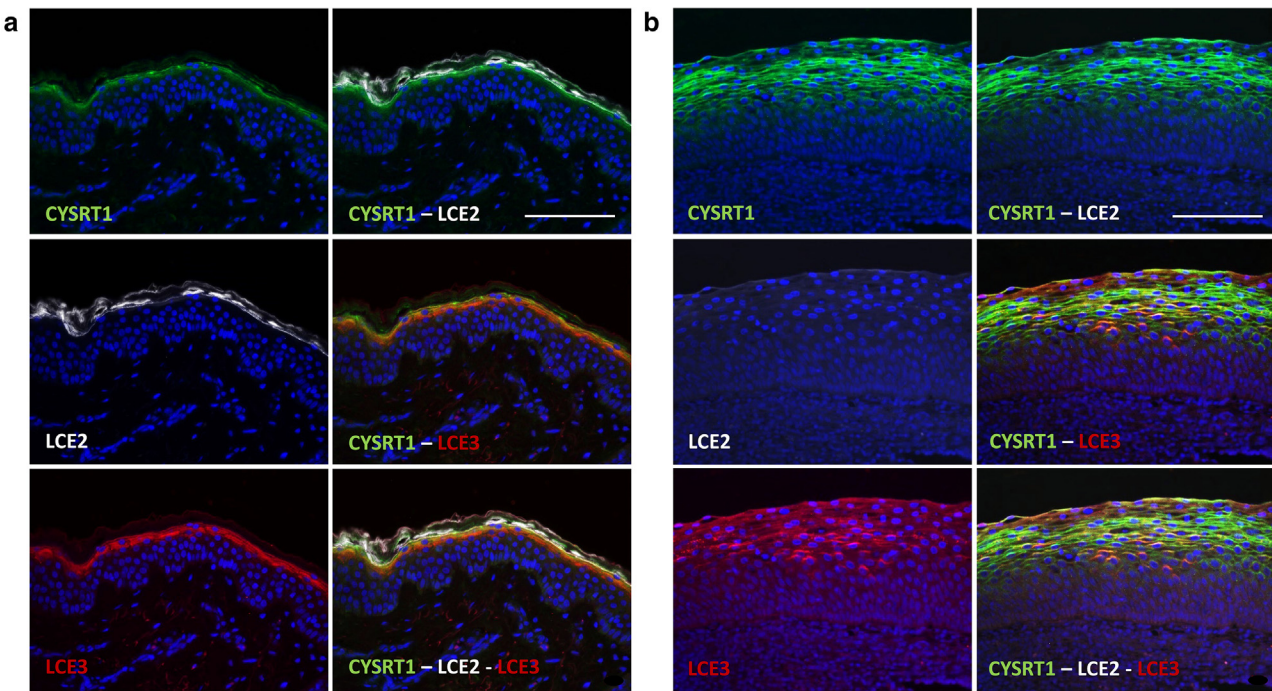




Supplementary Figure S4. Endogenously expressed CYSRT1 in keratinocyte cell extracts. Organotypic human epidermal equivalent generated from primary keratinocytes and *in vivo* interfollicular epidermal skin was lysed, and the protein extracts were analyzed by western blotting on a denaturing gel. Lane 1: precision plus protein standard dual color marker (Bio-Rad Laboratories, Hercules, CA). A strong band of endogenously expressed CYSRT1 is detected at 18–20 kDa using goat anti-CYSRT1 antibody in a human epidermal equivalent (lane 2) and in the interfollicular epidermis (lane 3).



Supplementary Figure S5. CYSRT1 protein expression in human skin. Variable CYSRT1 staining of stratum granulosum cells in skin biopsies from four healthy individuals. Continuous staining is seen in biopsy I and II, whereas discontinuous patchy staining is observed in the biopsies of individuals III and IV. Bar = 100 μ m.



Supplementary Figure S6. CYSRT1 colocalizes with LCE2 and LCE3. Immunofluorescence detection of LCE2 (white signal), LCE3 (red signal), and CYSRT1 (green signal) in (a) normal human skin and (b) tonsil epithelium. Nuclei are stained with DAPI (blue signal). Bars = 100 µm. LCE, late cornified envelope.

Supplementary Table S1. Positive Clones in Yeast-Two-Hybrid Screen with CYSRT1

| CYSRT1 Interaction Partner (HUGO Gene Name) | Number Identified Clones |
|---------------------------------------------|--------------------------|
| SKALP/elafin (<i>PI3</i>) | 3 |
| <i>DEFB4</i> | 2 |
| <i>K6</i> | 1 |
| LCE3A | 1 |
| <i>CNFN</i> | 1 |
| <i>BZW2</i> | 1 |
| <i>RACK1</i> | 1 |
| MALT1 paracaspase (<i>MALT1</i>) | 1 |

Abbreviations: HUGO, Human Genome Organisation; K6, keratin 6.

Supplementary Table S2. Primers Used for Cloning with the Gateway System

| Primer Name (Gene) | Primer Sequence (5' → 3') |
|--------------------------|-----------------------------------------------------|
| CYSRT1 FW | GGGGACAAGTTGTACAAAAAAGCAGGCTTCGACCCCCAAGAGATGGTCGTC |
| CYSRT1 REV | GGGGACCACTTGTACAAGAAAGCTGGTGCTAGGAGATGACACAGCAGCAG |
| LCE1A, 1C, 1D, 1E, 5A FW | GGGGACAAGTTGTACAAAAAAGCAGGCTTCCTCCAGCAGAGCCAGCAG |
| LCE1B, 3A, 3D FW | GGGGACAAGTTGTACAAAAAAGCAGGCTCTCCAGCAGAACAGCAG |
| LCE3B, 3E FW | GGGGACAAGTTGTACAAAAAAGCAGGCTCTGCCAGCAGAACAGCAG |
| LCE1F FW | GGGGACAAGTTGTACAAAAAAGCAGGCTCTGCCAGCAGAACAGCAG |
| LCE2A, LCE3C FW | GGGGACAAGTTGTACAAAAAAGCAGGCTCTCCAGCAGAACAGCAG |
| LCE2B, 2C, 2D FW | GGGGACAAGTTGTACAAAAAAGCAGGCTCTGCCAGCAGAACAGCAG |
| LCE4A FW | GGGGACAAGTTGTACAAAAAAGCAGGCTCTGCCAGCAGAACAGCAG |
| LCE6A FW | GGGGACAAGTTGTACAAAAAAGCAGGCTCTCACAGCAGAACAGCAG |
| LCE1A, 1D, 1E, 1F REV | GGGGACCACTTGTACAAGAAAGCTGGGTGTCAGCAGCAGCCTCAGAGTGC |
| LCE1B REV | GGGGACCACTTGTACAAGAAAGCTGGGTGCTCTAGGCTCAGGATCCACT |
| LCE1C REV | GGGGACCACTTGTACAAGAAAGCTGGGTGCTCTAGGCTCAGGTCAGGTCAG |
| LCE2A REV | GGGGACCACTTGTACAAGAAAGCTGGGTGCTGTGATGTTGAGGTCTGG |
| LCE2B REV | GGGGACCACTTGTACAAGAAAGCTGGGTGAGTTCTTAGGCCAGG |
| LCE2C REV | GGGGACCACTTGTACAAGAAAGCTGGGTGCTCTAGGCCAGG |
| LCE2D REV | GGGGACCACTTGTACAAGAAAGCTGGGTGCTCTGCAGGCCAGG |
| LCE3A REV | GGGGACCACTTGTACAAGAAAGCTGGGTGTCAGCAGCAGCCCCAGAACTG |
| LCE3B REV | GGGGACCACTTGTACAAGAAAGCTGGGTGGTAATTAGCATGTCAG |
| LCE3E REV | GGGGACCACTTGTACAAGAAAGCTGGGTGCTCAGCATCAGGATCTGGA |
| LCE3C REV | GGGGACCACTTGTACAAGAAAGCTGGGTGTCAGCAGCAGCCCCAGAGCCA |
| LCE3D REV | GGGGACCACTTGTACAAGAAAGCTGGGTGATCGCTGTCACTCAGGA |
| LCE4A REV | GGGGACCACTTGTACAAGAAAGCTGGGTGCTGCTCTGGCAG |
| LCE5A REV | GGGGACCACTTGTACAAGAAAGCTGGTGCTGCCTCATGGCCCAGG |
| LCE6A REV | GGGGACCACTTGTACAAGAAAGCTGGGTGACTGCACCTGTGCCTCA |

Abbreviations: FW, forward; REV, reverse.

Supplementary Table S3. Vectors Used for Cloning, Yeast Two-Hybrid, Coimmunoprecipitation, and Recombinant Protein Production

| Vector Name | Company | Tag | Purpose |
|------------------|--------------------------------------------------------------------------------------------|--------|-----------------------|
| pDONR201 | Gateway cloning, Life Technologies | — | Cloning |
| pGBK7 DNA-BD | Clontech | — | Yeast two-hybrid |
| pGADT7 AD | Clontech | — | Yeast two-hybrid |
| pcDNA3-HA/DEST | Provided by R. Roepman, Human Genetics Department, Radboudumc (Nijmegen, The Netherlands) | 3xHA | Coimmunoprecipitation |
| p3xFLAG-CMV/DEST | Provided by R. Roepman, Human Genetics Department, Radboudumc, (Nijmegen, The Netherlands) | 3xFLAG | Coimmunoprecipitation |